https://doi.org/10.1007/s41230-019-9013-x

Microstructure evolution of A380 aluminum alloy during rheological process under applied pressure

***Ying Wang[1], Shu-ming Xing[1], Xiao-hui Ao[2], and Ting-yue Wang[1]**

1. School of Mechanical, Electronic and Control Engineering, Beijing Jiaotong University, Beijing 100044, China

2. School of Mechanical Engineering, Beijing Institute of Technology, Beijing 100081, China

Abstract: In squeeze casting process, the essence of mold-filling and feeding is rheological solidification of the alloy melt under pressure. Microstructure evolution is inevitable in this process, which affects the mold-filling and feeding in turn. In this work, the Archimedes spiral sample prepared by indirect squeeze casting was applied to investigate the microstructure evolution during the rheological process under pressure. The results showed that the primary *α*-Al phase was transformed from fine rosette-like or granular structure to coarse platelet-like structure with the increase of spiral length. However, the primary *α*-Al grain size of the starting point had a slight growing trend compared with that at the position of 140 mm away from the starting point. The volume fraction of the primary *α*-Al phase increased from 45.57% to 70.35% along the spiral length direction, demonstrating that the experimental pressure improved the rheological ability of the alloy melt to some extent. Furthermore, the eutectic Si phase was varied from a fine granular or wormlike structure to a coarse platelet-like or needle-like structure, and the dispersion of eutectic Si particles was also varied along the spiral length direction. This microstructure evolution was mainly owing to the comprehensive action of rheological solidification and pressurized solidification. More specifically, the microstructure evolution strongly depended on the pressure and rheological velocity during the rheological process, however, the effect of rheological distance was relatively small.

Key words: microstructure evolution; primary α-Al; eutectic Si; rheological solidification; pressurized solidification

CLC numbers: TG146.21 **Document code:** A **Article ID:** 1672-6421(2019)06-371-09

Squeeze casting can be supposed as a combination of casting and forging [1, 2]. In this process, high pressure is applied to the melt during solidification to obtain fine grains. The essence of mold-filling and feeding is rheological solidification of the alloy melt under pressure. Microstructure evolution is inevitable in this process, which affects the mold-filling and feeding in turn. Therefore, research on microstructure evolution during the rheological process under applied pressure is extremely meaningful. A great deal of scientific research has been done on the mechanism of microstructure evolution[3-10]. The basic methods of refining microstructure are: controlling nucleation, inhibiting dendrites growth, and prompting the initial solidification nucleation [3]. Based on these ideas, various techniques, such as mechanical stirring [4], electromagnetic stirring [5], strain induced melt activation [6], casting using a cooling slope [7-9] and serpentine channel [3, 10] were used to generate the semisolid slurry with nearly spherical primary Al phase.

However, rheological behavior and stopping the rheological mechanism of liquid-solid alloy melt are relatively complicated. To solve those problems, many studies have been done, including qualitative studies on the rheological behavior of semisolid alloy melt [11-19] and quantitative studies by apparent viscosity [20]. Flemings et al. [11] found that when Sn-15wt.%Pb alloy was continuously cooled at a rate of 0.0055 $K \cdot s^{-1}$ under the condition of continuous shear, the apparent viscosity of semisolid alloy was low, and the primary solids were all spherical crystal without dendrites. Konijn [12] reported that the semisolid alloy melt behaved as a Newtonian fluid at the low solid fraction and had an obvious shear thinning characteristic at the high solid fraction. Defreit [13, 14] studied the rheological behavior of semisolid alloy melt by compressive testing, and the results showed that the rheological behavior exhibited pseudoplasticity in accordance with power-law relation. Liang [15] provided a model to investigate the origins of pseudoplasticity of semisolid metal slurries, and it was successfully applied to analyze the semisolid rheological behavior of magnesium alloy AZ91D. Lashkari [16]

***Ying Wang**

Female, born in 1987, Ph.D. candidate. Her research interest mainly focuses on feeding behavior of metals in squeeze casting.

E-mail: jyjdle@163.com

Corresponding author: Shu-ming Xing, E-mail: smxing@bjtu.edu.cn

Received: 2019-04-28; Accepted: 2019-08-11

studied alloy rheological behavior and microstructure via the viscosity. The results showed that the structure viscosity of dendrites, rose-crystals, and sphere-crystals successively decreased, and the viscosity difference was even raised an order of magnitude.

As is well-known, the nucleation rate is the most important parameter during the rheological process of semisolid alloy. The dendritic network is broken by increasing the shear stress on the grain or enhancing the fluctuating state of the alloy melt, thereby forming more crystal nuclei. The broken dendritic structures collide with each other to obtain the fine and round microstructure. Many researchers have proved that the feeding flow can alter the morphology of microstructures [21-23]. In order to promote the research of rheological feeding in squeeze casting, the microstructure evolution of alloy melt during the rheological process under applied pressure should be further studied.

Based on the previous studies, it can be seen that the key factors of microstructure evolution are the pressure applied onto alloy melt, and the rheological velocity during solidification [21-23]. The purpose of rheological squeeze casting is to obtain a fine microstructure by making full use of pressure and shear scour actions during the rheological process. To increase the length of the rheological path, the Archimedes spiral sample prepared by indirect squeeze casting was applied to investigate microstructure evolution during the rheological process under pressure by comparing microstructures at different positions along the length direction of the spiral line.

1 Experimental

1.1 Sample preparation

This experiment was conducted using the spiral mold designed by our semi-solid forming laboratory, as shown in Fig. 1. There are four main parts of the mold including upper die, lower die, punch, and chamber. The upper die cavity is the Archimedes spiral line with a total length of 1,350 mm and a square cross section with 8 mm in side length. The lower die is a cylindrical chamber, which connects with the Archimedes spiral cavity by the runner on the side wall.

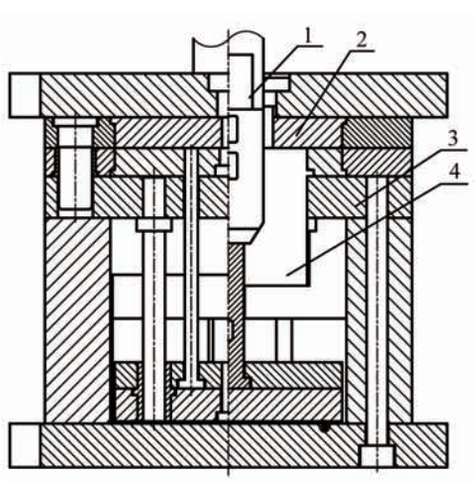

Fig. 1: Mold of spiral sample: 1-punch; 2-upper die; 3-lower die; 4-chamber

A380 aluminum alloy applied in this work has good fluidity, good mechanical properties and high Si content, whose chemical compositions are shown in Table 1. The solidus and liquidus temperatures of this alloy are 525 °C and 596 °C [3], respectively.

Table 1: Chemical compositions of A380 alloy (wt.%)

Si	Cu	Fe	Zn	Mn	Ce	Mg	Ni	Sn	Al
8.313	3.394	0.767	0.915	0.407	0.430	0.081	0.049	0.054	Bal.

Indirect squeeze casting was applied. The alloy was melted in an electrical furnace of 5 kW, and the temperature was measured by TES-1310 type contact thermometric instruments and K type thermocouples. When the melt temperature reached 720 ± 5 °C, CCl_4 (0.2% weight of alloy) was added to refine the alloy melt. Ten minutes later, it was slagged off. The alloy liquid was allowed to stand, and when the temperature was adjusted to 720 °C, it was directly poured into the lower die with a preheated temperature of 170 °C. Upper and lower dies were closed. Then the punch moved down, driven by the filling cylinder (30 $mm \cdot s^{-1}$) to squeeze the alloy melt back into the cavity. Pressure holding at 120 MPa for 20 s, the punch was reset. The pressure was removed from the movable beam, which drove the upper die to reset. Lastly, the sample was ejected out of the mold by ejectors.

1.2 Test method

Six microstructural analysis samples of A (starting point), B (140 mm away from the starting point), C (340 mm away from the starting point), D (540 mm away from the starting point), E (740 mm away from the starting point) and F (ending point, i.e., 840 mm away from the starting point) were selected from the spiral line, as shown in Fig. 2. The samples were ground with grinding paper ranging from 320 to 2000 grits and polished with 1.5 μm alumina, then were ultrasonically cleaned and etched using Keller reagent. Each sample was observed at the center using the DM2000 optical microscope (OM) and ZEISS EVO.18 scanning electron microscope (SEM).

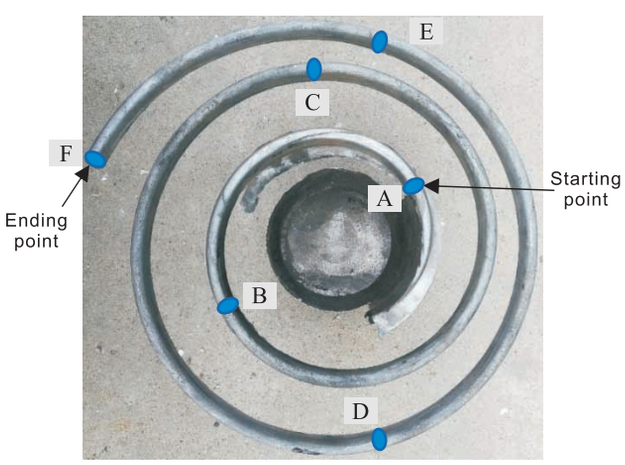

Fig. 2: Spiral sample

Quantitative metallographic analysis was executed according to GB/T 15749-2008. The metallographs were imported into Image-Pro Plus software for image collection, analysis, and quantitative calculation. The area and perimeter of grain were measured by Image-Pro Plus 6.0 software. Average grain diameter D can be defined as Eq. (1):

$$D = \frac{1}{m}\sum_{j=1}^{m}\left[\frac{1}{n}\sum_{i=1}^{n} 2\left(A_i/\pi\right)^{0.5}\right] \quad (1)$$

Grain shape factor F can be defined as Eq. (2):

$$F = \frac{1}{m}\sum_{j=1}^{m}\left[\frac{1}{n}\sum_{i=1}^{n} 4\pi A_i/P_i^2\right] \quad (2)$$

where m is the number of view fields; n is the number of primary α-Al grains; A_i denotes the area of primary α-Al grains; P_i represents the perimeter of primary α-Al grains, respectively. In order to increase the reliability of quantitative calculation, each sample was captured in 10 view images using an optical microscope, and 10 α-Al grains were measured in every view.

2 Results

2.1 Variation of primary α-Al phase morphology and size along spiral length direction

The total length of the spiral sample was 840 mm by indirect squeeze casting in this work. The optical microstructures of different positions along the spiral length direction are displayed in Fig. 3. The bright granules are the primary α-Al grains and the dark zones are the eutectic microstructures derived from the remaining liquid. The result indicates that the primary α-Al phase is transformed from fine rosette-like or granular structure to coarse platelet-like structure with the increase of spiral length. Of special note, the primary α-Al phase at the position of 140 mm away from the starting point is more round, as shown in Fig. 3 (b). However, the grain size of the starting point has a slight growing trend compared with that of the 140 mm position, as presented in Fig. 3 (a), i.e., the average diameter at the staring point is 22.9 μm , and that at the 140 mm position is 17.81 μm , as shown in Fig. 4. This phenomenon is mainly due to the fact that the starting point has the highest temperature and is the last location to solidify, thus the alloy melt has enough time to grow up. However, the pressure and rheological speed are the maximum at the starting point, limiting the growth of grains [22-24]. The effect of temperature on the grain size is greater than that of pressure and rheological speed at the range of 140 mm from the starting point. Thus, the grains of the starting point have a slight trend of growing up eventually.

The evaluation of primary α-Al phase shape factor and average diameter along the spiral length direction was performed using a digital image analyzer system. The quantitative results are exhibited in Fig. 4, which shows that the primary α-Al phase shape factor increases from 0.5669 for the starting point to 0.659 for the 140 mm position, then gradually decreases to 0.3801 for the ending point; and the average diameter reduces from 22.9 μm for the starting point to 17.81 μm for the 140 mm position, and then gradually rises to 44.58 μm for the end point.

2.2 Variation of primary α-Al phase volume fraction along spiral length direction

The variation of the primary phase volume fraction along the spiral length direction is presented in Fig. 5, which shows that the primary α-Al phase volume fraction increases from

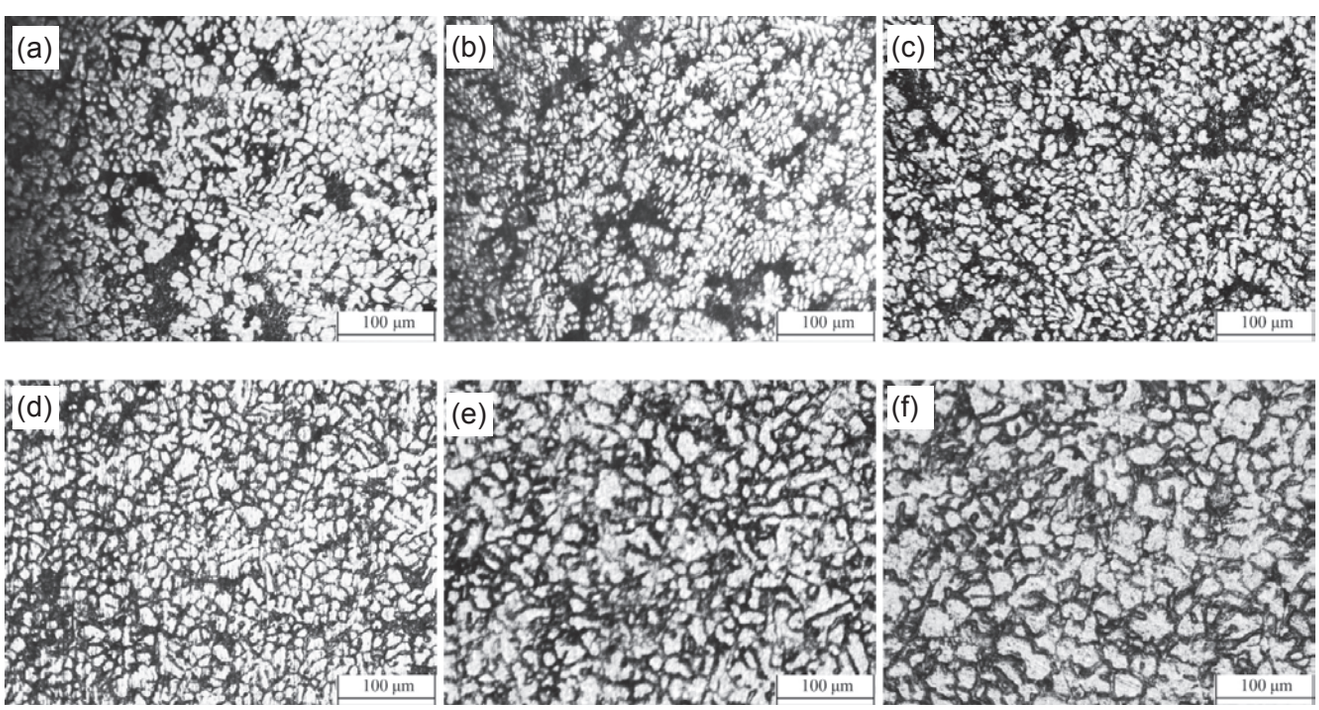

Fig. 3: Optical microstructures along spiral length direction: (a) starting point ; (b)140 mm ; (c) 340 mm ; (d) 540 mm; (e) 740 mm ; (f) 840 mm

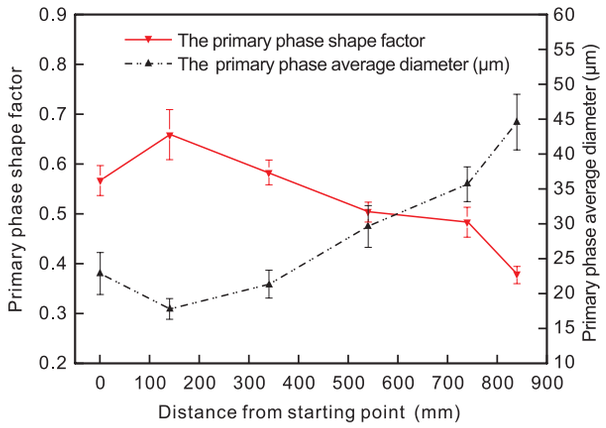

Fig. 4: Variation of primary α-Al phase shape factor and average diameter along spiral length direction

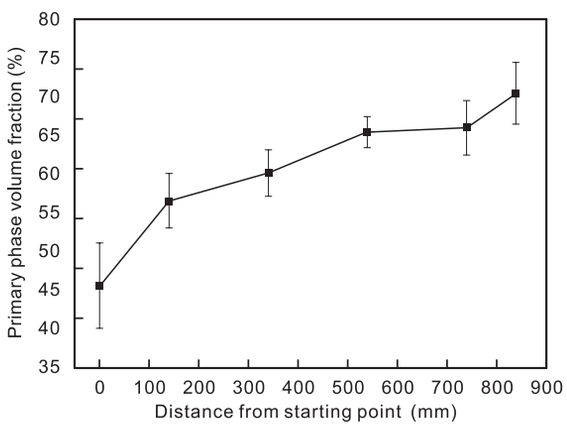

Fig. 5: Variation of primary α-Al phase volume fraction along spiral length direction

45.57% to 70.35%. The reason for this phenomenon may be that the liquid phase of the final filling cavity has a high solute concentration due to the fact that the alloy melt in contact with the ejector is the first to solidify caused by the rapid cooling.

Figure 6 also shows that when the rheological solid fraction is up to 70.35%, the alloy slurry loses its fluidity. However, when the solid volume fraction is more than 60%, the feeding pressure loss sharply increases, as shown in Fig. 6 [25]. The maximum packing point may be reached at the 60% solid volume fraction. Thus, the pressure applied in this work improved the rheological ability of the alloy melt to some extent. At the beginning of the solidification, the primary solid phase dispersed in the liquid phase and grew up independently. With the solidification proceeding, crystal overlapped with each other and formed a mesh structure with certain intensity. When the mesh structure strength reached to material rheological shear stress, the alloy melt lost the rheological ability. However, the pressure applied in the squeeze casting process destroyed the mesh structure, and the alloy melt continued to flow, thereby increasing the rheological ability of alloy melt.

2.3 Variation of eutectic Si phase morphology and size along spiral length direction

Due to the existing Al-Si-Al_2Cu ternary eutectic in A380

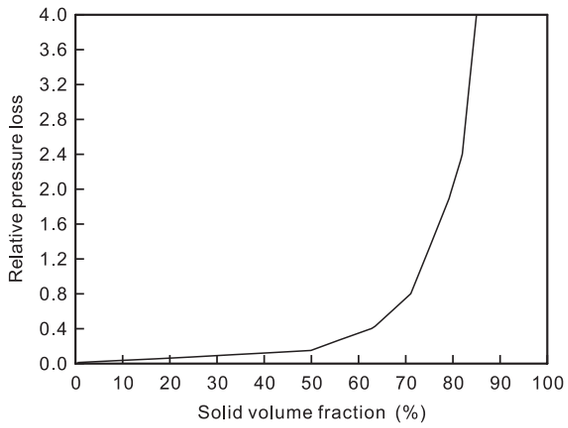

Fig. 6: Variation of relative pressure loss with solid volume fraction [25]

aluminum alloy, the EDS area scans and point scans for SEM image at the 140 mm position (Point B in Fig. 2) were conducted to distinguish eutectic Si and Al_2Cu, as shown in Fig. 7. It can be seen that the granular or wormlike structure with reticulate distribution is eutectic Si according to Fig. 7(a), (b) and (d), and the bright white phase along grain boundary is Al_2Cu according to Fig. 7(a), (c) and (e).

Figure 9 shows SEM images of the microstructure along the spiral length direction, in which the dark zones are the primary α-Al phases and the bright structures are the eutectic Si microstructures derived from the remaining liquid. The result presents that the eutectic Si phase varies from a fine granular or wormlike structure to a coarse platelet-like or needle-like structure, and the dispersion of eutectic Si particles also varies along the spiral length direction. From the starting point to the 340 mm position [as shown in Fig. 8(a)–(c)], the eutectic silicon distribute as reticular structure, while the size of eutectic Si particles gradually increases. However, comparing Fig. 8(c) with Fig. 8(d), the morphology of eutectic Si evidently varies from granular to platelet-like or needle-like. From the 540 mm position to the ending point [as shown in Fig. 8(d)–(f)], the size of the platelet-like or needle-like eutectic structure is transformed from fine to coarse.

3 Discussion

Because of the chilling effect of the inner wall and the punch, and the heat dissipation of the surface, a solidified shell is formed before the alloy melt is poured into the cavity of the spiral line. Therefore, the alloy melt can be considered as the semi-solid alloy melt, and its rheological characteristic is strongly dependent on the solid volume fraction, and has the characteristic of Bingham fluid [26]. When the shear stress is less than the yield limit, the melt has a solid characteristic without fluidity. However, when the shear stress is greater than or equal to the yield limit, the melt may start to flow.

On one hand, the yield limit increases with the increase of the primary α-Al phase volume fraction from the starting point to the ending point (as shown in Fig. 4). On the other hand, the pressure decreases with the increase of the rheological

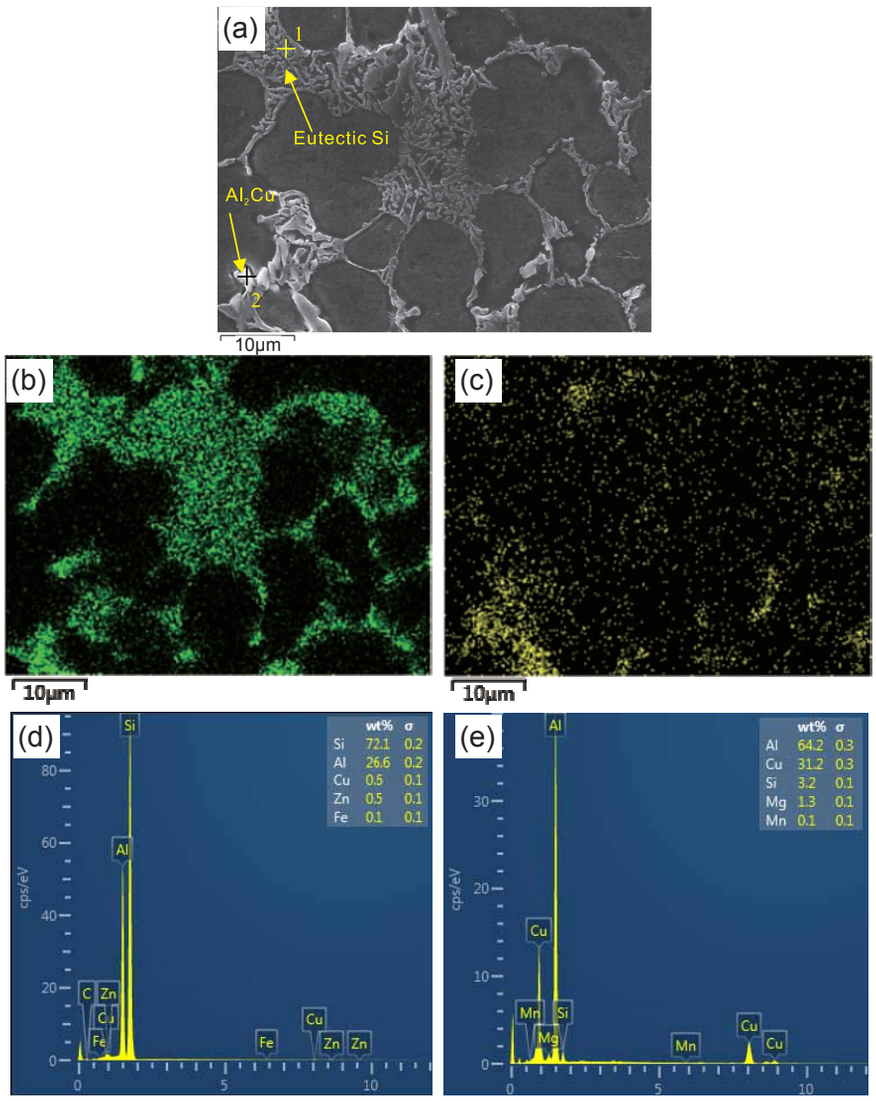

Fig. 7: SEM and EDS images at 140 mm position: (a) SEM; (b and c) EDS area scans of image (a); (d and e) EDS point scans of Point 1 and Point 2

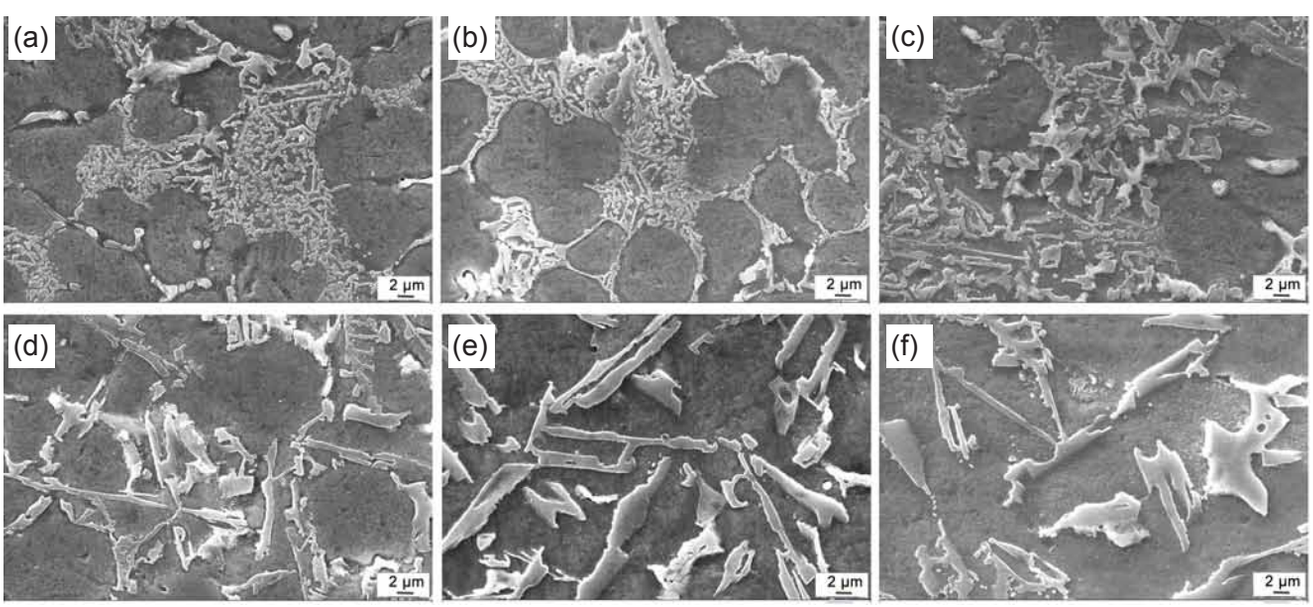

Fig. 8: SEM images of microstructure along spiral length direction: (a) starting point ; (b)140 mm ; (c) 340 mm; (d) 540 mm ; (e) 740 mm ; (f) 840 mm

distance. These two aspects lead to the shear rheological effect gradually decreasing from the starting point to the ending point, even though there is no shear rheological velocity at the ending point. Therefore, the primary α-Al grain varies from fine and round to coarse and irregular with the increase of distance from the starting point, as shown in Fig. 3, and eutectic Si phase varies from a fine granular or wormlike structure to a coarse platelet-like or needle-like structure, as shown in Fig. 8.

3.1 Rheological solidification - one mechanism of microstructure evolution

The results of microstructure evolution can be analyzed from the perspective of rheological solidification. The tiny unit schematic of the spiral sample is shown in Fig. 9. Tiny units, α and β, firstly flow into the spiral line and eventually flow to the end of α' and β', respectively. Taking α and β for analysis, the solid particles in the semisolid alloy melt roll over and collide with each other, thus the primary solid phase becomes small [3, 9, 19, 22, 23]. Along the spiral length direction, the microstructure evolution mechanism of rheological solidification is mainly affected by rheological velocity and rheological distance. These two aspects are similar to slope length and angle described in literature [9], respectively.

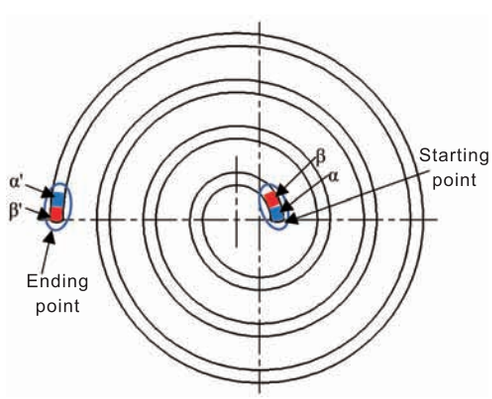

Fig. 9: Tiny unit schematic of spiral sample

From the perspective of rheological velocity, the velocity of tiny unit β is always less than that of α, due to the energy loss which should not be neglected in the process of delivery. In other words, the rheological velocity gradually decreases with the increase of rheological distance. The rolling or colliding of solid particles in the alloy melt is gradually weakened. The lower shear forces acting on the solidifying melt cannot transform the dendritic morphology into the globular form of the primary α-Al phase [27-28]. Therefore, the closer the tiny unit is away from the starting point, the finer the microstructures.

From the perspective of rheological distance, the distance of tiny unit β is always greater than that of α. With the increasing of rheological distance, the rolling and colliding among particles is intensifying, leading to the uniform fine microstructures. However, the greater amount of solid fraction is obtained when the rheological distance is beyond a certain value, which results in the semi-solid alloy melt losing its fluidity. This in turn coarsens the primary α-Al phase [29].

It can be seen from Fig. 3 and Fig. 4 that the finest grain is located at the 140 mm position rather than at the ending point, due to the effect of fluctuation intensity on structure refinement. The Archimedes spiral sample prepared in this work ingeniously used the semisolid rheological forming principle. The feeding punches extruded alloy melt back into the cavity during the squeeze casting process. The melt experienced the rheological extrusion before entering the spiral cavity. The microstructures were refined by the alloy melt rheological solidification under high pressure. Studies have shown that the rheological solidification structures are closely related to the fluctuation intensity of alloy melt [30-31]. With the increase of rheological distance, the rheological rate of alloy melt is reduced because of the energy consumption caused by rheological resistance. The flow velocity is relatively high near the starting point. Under the strong shear rheology, the dendrites are sheared into fragments, eventually evolving into non-dendritic primary phase [25, 33], as shown in Fig. 10.

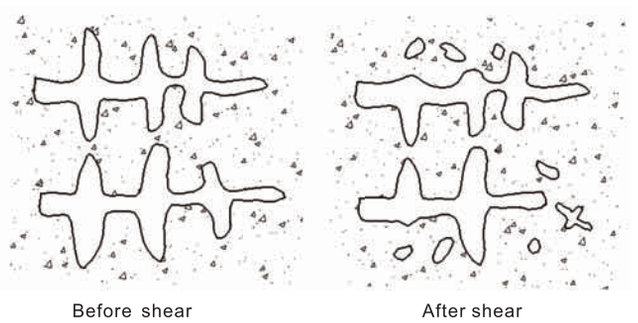

Fig. 10: Schematic of dendrite shearing into fragments [33]

At the same time, in the process of dendrite growth, the liquid solidification temperature around the dendrite root reduces due to the emissions and enrichment of solute, which prevents the solid phase of the root from growing. Therefore, the radius of the dendritic root is always less than that of the top. Under strong shear rheology, it is easy to produce the necking and remelting of the dendrite root, as shown in Fig. 11. Similarly, concentrations of the solute in the liquid phase near the dendrite arm are different due to the difference of curvature of the secondary dendrite arm. The smaller the radius of curvature, the lower its nearby liquid solute concentration, resulting in a concentration gradient of the solute. This gradient induces the solute to diffuse from the coarser branches to the thinner ones, which causes the dendrite merging growth phenomenon of twigs melting and thick branches becoming coarse [8, 32].

However, nucleus growth control theory of the semisolid non-dendritic primary phase is more reasonable in explaining the special roundness of grain structure at 140 mm position from the starting point. Under the condition of shear rheology, temperature and solute boundary layer thickness reduce, and the growth of the dendrite arm tip is promoted through the shear infiltration into the melted part of the solute enrichment among the secondary dendritic arms. However, the shear has little impact on the growth of the dendrite arm root, thus

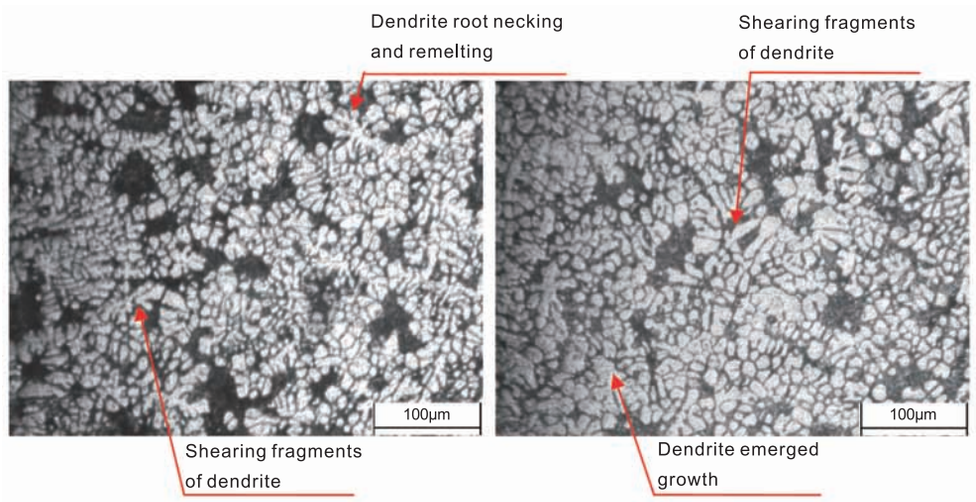

Fig. 11: Dendrite degradation during rheological process under applied pressure

forming the rosette primary phases [34]. Under the condition of high flow velocity, turbulent flow is generated and further penetrates into the secondary dendrite arm. The thinner boundary layer caused by high turbulence intensity, the reduction of composition undercooling, and the capillary effect all help to improve the growth rate of the dendrite arm root and inhibit the formation of rosette primary phase. When the flow velocity is high enough, the primary phase will continue to keep the globular crystal growing [35].

In summary, the rheological solidification of metal is a complex dynamic process during the squeeze casting process, thus its refinement mechanism is also the result of the comprehensive action of multiple mechanisms. According to the above analysis, the refinement mechanism of rheological solidification may include dendrite shearing to fragments, dendrite root necking and remelting, dendrite emerged growth, recrystallization refinement, and nucleus growth control theory of the non-dendritic primary phase.

3.2 Pressurized solidification - another mechanism of microstructure evolution

Take two tiny units α and β (Fig. 9) for analysis. In the solidification process, the pressure of tiny unit β is transferred from that of α. The pressure of tiny unit β is always less than that of α due to the fact that applied pressure needs to overcome materials viscous force and frictional resistance of the mold wall. So, from the perspective of pressurized solidification, the closer to the starting point, the greater the pressure acting on the alloy melt. The solidification structure will become finer under greater pressure action [33].

Squeeze casting is a process of alloy melt solidification under pressure. Applied pressure needs to overcome the rheological resistance of the materials, thus the pressure gradually attenuates with the increase of rheological distance. This phenomenon is further analyzed through the loss of feeding pressure [25]. The feeding channel of the solidification process is supposed to be a capillary model. Punch pressure is largely greater than alloy melt gravity. Ignoring the action of gravity, the loss of feeding pressure p_f can be expressed by Eq. (3) [25]:

$$p_f = \frac{f_s^2}{8\left(1-f_s\right)^2}\frac{Cp}{\eta n \pi L_m} \tag{3}$$

where f_s is the solid fraction of alloy melt ($0 < f_s < 1$), C is a coefficient associated with dendrite arm spacing, p is the applied pressure, η represents dynamic viscosity of alloy melt, L_m is the capillary length, n is the number of feeding channels per unit area.

It can be seen from Eq. (3) that the pressure loss p_f is increased with the increase of solid fraction f_s; and the higher the solid fraction, the faster the growth rate of pressure loss. During the squeeze casting process, the temperature of the alloy melt gradually reduces with the increase of feeding flow distance, while solid fraction f_s gradually increases, which results in the rapid increase of pressure loss. It can be seen from Fig. 3 and Fig. 4 that microstructure morphologies and sizes in the different positions have significant changes along the spiral length direction, indirectly reflecting the effect of the pressure attenuation on microstructure. The greater the pressure, the finer the microstructure.

There are two kinds of grain refinement mechanisms which are widely accepted by the researchers during the pressurized solidification process. One mechanism is that the pressure affects the alloy melting point [1], which mainly considers the influence of pressure on the alloy phase diagram, as shown in Fig. 12. The Clausius–Clapeyron equation is as follows:

$$\frac{\Delta T_f}{\Delta p} = \frac{T_f\left(V_l - V_s\right)}{\Delta H_f} \tag{4}$$

where T_f represents equilibrium solidification temperature of the alloy, V_l and V_s denote the volume of liquid and solid, respectively, and ΔH_f is the specific heat capacity.

As can be seen from Eq. (4) and Fig. 12, the application of pressure brings about undercooling in an initially superheated alloy and thus can effectively promote the nucleation rate, so refining the solidification structure.

Another mechanism is that the pressure can affect the heat

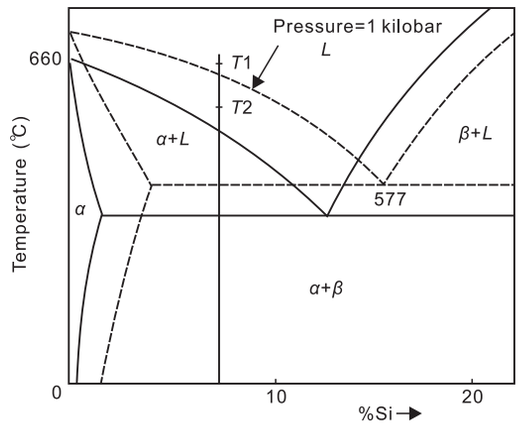

Fig. 12: Application of pressurized solidification on Al-Si phase diagram [1]

transfer coefficient between the casting and the mold. In the traditional casting process, the overheated alloy melt is poured into the mold cavity. Firstly, a layer solidified shell is formed in the surface due to solidification shrinkage. Thus, a thin layer gas gap is generated between the mold cavity surface and solidified shell, significantly influencing the heat transfer mechanism between the casting and mold, resulting in the heat transfer mode transforming from liquid→solid to solid→gas→solid. Due to the fact that the thermal conductivity of the gas is far lower than that of the liquid and solid, the gas gap seriously reduces the heat transfer coefficient between casting and mold, which reduces the cooling rate of castings. Therefore, the grains become coarse. Improving the cooling rate, on the one hand, can quickly release latent heat so as to improve the survival rate of the heterogeneous nucleus; on the other hand, it can limit the grain growth in the solidification process. The entire solidification process takes place under pressure during the squeeze casting process, thus the gas gap between the mold cavity surface and the solidified shell is gradually reduced until it disappears. The heat transfer coefficient is greatly increased because the heat transfers from solid to solid, which is equivalent to increasing the cooling rate. Thus, the fine as-cast structure is obtained.

It is difficult to distinguish the two kinds of mechanism during the squeeze casting process, due to the limitation of the existing theory and experimental conditions. That is to say, two refinement mechanisms have an effect on the final solidification structure at the same time. However, only one mechanism plays a leading role in refining the microstructure at different times and under different conditions. The results [1] show that initially pressurized time is the key factor in contributing to the refinement of the final solidification structure. If the temperature of the alloy melt is higher at the initially pressurized time, the pressure suppresses the production of the gas gap, thus increasing the heat transfer coefficient between casting and mold. At this moment, pressure has less effect on the alloy melting point, however, the effect of pressure on the heat transfer coefficient plays a leading role. On the other hand, if initially pressurized time is relatively late, a thin gas gap has formed. At this moment, pressure has less effect on the heat transfer coefficient, however, the effect of pressure on the alloy melting point plays a leading role.

4 Conclusions

This work was devoted to studying the microstructure evolution of A380 aluminum alloy during the rheological process under applied pressure. The results can be summarized as follows:

(1) The primary α-Al phase was transformed from fine rosette-like or granular structure to coarse platelet-like structure with the increase of spiral length. However, the primary α-Al grain size of the starting point had a slight growing trend compared with that at the position of 140 mm from the starting point.

(2) The volume fraction of the primary α-Al phase increased from 45.57% to 70.35% along the spiral length direction. The stopping rheological solid fraction was as high as 70.35%, which demonstrated that the experimental pressure improved the rheological ability of alloy melt.

(3) The eutectic Si phase varies from a fine granular or wormlike structure to a coarse platelet-like or needle-like structure, and the dispersion of eutectic Si particles was also varied along the spiral length direction.

(4) The microstructure evolution from fine to coarse along the spiral length direction was mainly owing to the result of the comprehensive action of rheological solidification and pressurized solidification. More specifically, microstructure evolution strongly depended on the pressure and rheological velocity during the rheological process under pressure, however, the effect of rheological distance was relatively small.

Future work will focus on the research of the morphology and size of second phase particles including θ-phase (Al_2Cu), α-phase ($Al_{15}(Fe, Mn)_3Si_2$) and β-phase (Al_5FeSi) during the rheological process under applied pressure.

References

[1] Ghomashchi M R, and Vikhrov A. Squeeze casting: an overview. J. Mater. Process Technol., 2000, 101 (1-3): 1–9.
[2] Maleki A, Niroumand B, and Shafyei A. Effects of squeeze casting parameters on density, macrostructure and hardness of LM13 alloy. Mater. Sci. Eng. A, 2006, 428(1-2): 135–140.
[3] Liu Z Y, Mao W M, Wang W P, et al. Preparation of semi-solid A380 aluminum alloy slurry by serpentine channel. Trans Nonferrous Met Soc China, 2015, 25(5): 1419–1426.
[4] Alvani S M J, Aashuri H, Kokabi A, et al. Semisolid joining of aluminum A356 alloy by partial remelting and mechanical stirring. Trans. Nonferrous Met. Soc. China, 2010, 20(9): 1792–1798.
[5] Liu Z, Mao W M, and Liu X M. Characterization on morphology evolution of primary phase in semisolid A356 under slightly electromagnetic stirring. Trans. Nonferrous Met. Soc. China, 2010, 20(s3): 805–810.
[6] Wannasin J, Martinez R A, and Flemings M C. Grain refinement of an aluminum alloy by introducing gas bubbles during solidification. Scripta Mater., 2006, 55(2): 115–118.
[7] Gencalp S, and Saklakoglu N. Semisolid Microstructure Evolution during Cooling Slope Casting under Vibration of A380 Aluminum Alloy. Mater. Manuf. Processes, 2010, 25(9): 943–947.

[8] Das P, Kumar M, Samanta S K, et al. Semisolid Processing of A380 Al Alloy Using Cooling Slope. Mater Manuf Processes, 2014, 29(4): 422–428.
[9] Mandal S K, Mandal N, Roy H, et al. Optimization of processing parameters of cooling slope process for semi-solid casting of ADC 12 Al alloy. J. Braz. Soc. Mech. Sci. Eng., 2018, 40(6): 291–305.
[10] Liu Z Y, Mao W M, Wang W P, et al. Investigation of rheo-diecasting mold filling of semi-solid A380 aluminum alloy slurry. Int. J. Miner., Metall. Mater., 2017, 24(6): 691–700.
[11] Flemings M C. Behavior of metal alloys in the semisolid state. Metall. Trans. A, 1991, 22(3): 269–293.
[12] Konijn B J, Sanderink O B J, and Kruyt N P. Experimental study of the viscosity of suspensions: Effect of solid fraction, particle size and suspending liquid. Powder Technol., 2014, 266(6): 61–69.
[13] De Freitas E R, Ferracini E, and Ferrante A. Microstructure and rheology of an AA2024 aluminium alloy in the semi-solid state, and mechanical properties of a back-extruded part. J Mater Process Technol., 2004, 146(2): 241–249.
[14] Ferrante M, and de Freitas E. Rheology and microstructural development of a Al–4wt%Cu alloy in the semi-solid state. Mater. Sci. Eng. A, 1999, 271(1–2): 172–180.
[15] Li L, Zheng M. Theoretical research on rheological behavior of semisolid slurry of magnesium alloy AZ91D. Comput. Mater. Sci., 2015, 102: 202–207.
[16] Lashkari O, and Ghomashchi R. The implication of rheological principles for characterization of semi-solid Al–Si cast billets. J. Mater. Sci., 2006, 41(18): 5958–5965.
[17] Qi M F, Kang Y L, Zhou B, et al. A forced convection stirring process for Rheo-HPDC aluminum and magnesium alloys. J. Mater. Process Technol., 2016, 234: 353–367.
[18] Parshizfard E, and Shabestari S G. An investigation on the microstructural evolution and mechanical properties of A380 aluminum alloy during SIMA process. J. Alloys Compd., 2011, 509(40): 9654–9658.
[19] Zheng Z K, Ji Y J, Mao W M, et al. Influence of rheo-diecasting processing parameters on microstructure and mechanical properties of hypereutectic Al–30%Si alloy. Trans. Nonferrous Met. Soc. China, 2017, 27(6): 1264–1272.
[20] Liu W. Study on apparent viscosity of semi-solid alloy melt. PhD Dissertation, 2007, Beijing Jiaotong University, Beijing.
[21] Wang F F, Ma Q X, Meng W, et al. Experimental study on the heat transfer behavior and contact pressure at the casting-mold interface in squeeze casting of aluminum alloy. Int. J. Heat Mass Transfer, 2017, 112: 1032–1043.
[22] Steinbach S, Ratke L. The Influence of Fluid Flow on the Microstructure of Directionally Solidified AlSi-Base Alloys. Metall. Mater. Trans. A, 2007, 38(7): 1388–1394.
[23] Ren Z M, Jin J Z, and Guo K R. Effect of fluid flow on dendritic structure of Al-Si alloy. J. Mater. Sci., 1991, 26(13): 3599–3602.
[24] Hao L Y, Yang X, Lu S L, et al. Influence of squeeze casting pressure and heat treatment on microstructure and mechanical properties of Mg94Ni2Y4 alloy with LPSO structure. Mater. Sci. Eng. A, 2017, 707: 280–286.
[25] Xiong B W, Lin X, Wang Z J, et al. Microstructures and mechanical properties of vacuum counter-pressure casting A357 alloys solidified under grade-pressurising: effects of melt temperature. Mater. Sci. Eng. A, 2014, 611(31): 9–14.
[26] Tan J B, Xing S M, Li L X, et al. Limiting length of semi-solid A356 alloy rheological filling. Chin. J. Nonferrous Met., 2006, 16(6): 970–975.
[27] Guan R G, Cao F R, Chen L Q, et al. Dynamical solidification behaviors and microstructural evolution during vibrating wavelike sloping plate process. J. Mater. Process Technol., 2009, 209(5): 2592–2601.
[28] Saklakoglu N, Gencalp S, Kasman S, et al. Formation of globular microstructure in A380 aluminum alloy by cooling slope casting. Adv. Mater. Res., 2011, 264–265: 272–277.
[29] Liu W, Tan J B, Li J.Q., et al. Influence of process parameters by vibrational cooling-shearing slope on microstructures of semi-solid ZAlSi9Mg alloy. Adv. Mater. Res., 2011, 211–212: 142–146.
[30] Xiu H, Huang C M, Bai H W, et al. Improving impact toughness of polylactide/poly(ether)urethane blends via designing the phase morphology assisted by hydrophilic silica nanoparticles. Polym., 2014, 55(6): 1593–1600.
[31] Lus H M, Turkeli A, and Kinikoglu NG. Swage casting of A380 alloy. Mater. Des., 2011, 32(6): 3570–3577.
[32] Hu H Q. Metal solidification principle 2nd edn. Mechanical Industry Press, 2000, Beijing.
[33] Zhang Y. Study on microstructure and mechanical behavior of rheo-squeeze casting AZ91-Ca alloys. Ph.D Dissertation, 2015, Shanghai Jiao Tong University.
[34] Das A, and Fan Z. A Monte Carlo simulation of solidification structure formation under melt shearing. Mater Sci Eng A, 2004, 365(1–2): 330–335.
[35] Das A, Ji S, and Fan Z. Morphological development of solidification structures under forced fluid flow: a Monte-Carlo simulation. Acta Mater., 2002, 50(18): 4571–4585.

This work was financially supported by the National Natural Science Foundation of China (No. 51275031).